Ore Geology Reviews 144 (2022) 104837

Contents lists available at ScienceDirect

Ore Geology Reviews

journal homepage: www.elsevier.com/locate/oregeorev

Zircon Th/U ratios suggest a post-collision extensional setting for the Permian Ni-Cu sulfide deposits in the Eastern Tianshan, NW China

Wei Xie [a,b,*], Yin Lu [a], Lie-Meng Chen [c,*], Xie-Yan Song [c], Yu-Feng Deng [d], Yun Zhao [e]

[a] Key Laboratory of Marine Hazards Forecasting, Ministry of Natural Resources (MNR), College of Oceanography, Hohai University, Nanjing 210098, China
[b] Southern Marine Science and Engineering Guangdong Laboratory (Guangzhou), Guangzhou 511458, China
[c] State Key Laboratory of Ore Deposit Geochemistry, Institute of Geochemistry, Chinese Academy of Sciences, Guiyang 550081, China
[d] Ore Deposit and Exploration Center (ODEC), Hefei University of Technology, Hefei 230009, China
[e] State Key Laboratory of Geological Processes and Mineral Resources, China University of Geosciences, Beijing 100083, China

ARTICLE INFO

Keywords:
Zircon Th/U ratios
Ni-Cu sulfide deposits
Eastern Tianshan
Post-collision extensional setting

ABSTRACT

Magmatic Ni-Cu sulfide deposits have been discovered in orogenic belts worldwide. However, the optimal period for extensive basaltic magmatism generating Ni-Cu sulfide mineralization during the development of orogenic belts has not been well addressed. Zircon Th/U may be correlated with end-member tectonic stress regimes (continental extension vs. compression) that correlate with distinct magmatic conditions. Here, zircon Th/U ratios from the Permian Huangshan-Jingerquan Ni-Cu metallogenic belt in the Eastern Tianshan are revisited, including magmatic zircons from mafic and felsic rocks and detrital zircons from sedimentary rocks. These zircons are filtered to minimize the effect of amagmatic conditions (e.g., metamorphism, alteration, inclusion and metamictization). After filtration, zircon Th/U ratios in the Huangshan-Jingerquan belt are likely linked to the silica content of the host melt and crystallization temperature under zircon growth with fractionating melts. They display high Th/U ratios (up to 2.5) and δEu values (up to 1.35) during the early Permian. In contrast, the others with low Th/U (most < 1.0) ratios and δEu (<0.8) appear in the pre-Permian except the late Devonian. This indicates that the crust in the region was thickened induced by collision at the end of late Carboniferous and then extended during the early Permian. Conclusively, we suggest that the post-collision extensional setting is the preferred stage for the Permian short-lived (<5 Ma) Ni-Cu sulfide deposits during the development of the Tianshan Orogenic Belt.

1. Introduction

Economic Ni-Cu sulfide deposits and sulfide mineralization hosted by mafic-ultramafic complexes have been discovered in orogenic belts worldwide in recent decades. Although these deposits contain less than 10% of the total nickel metal reserves in the world, they contain ~ 34% of the total Ni metal reserves in China (e.g., Zhou et al., 2004; Deng et al., 2014; Mao et al., 2016, 2018; Zhao et al., 2018b; Song et al., 2021), including the giant Xiarihamu Ni-Co deposit in the East Kunlun Orogenic Belt (e.g., Song et al., 2016; Liu et al., 2018), the Lengshuiqing deposit along the western margin of the Yangzi Block (Yao et al., 2018), and the Huangshan-Jingerquan belt and the Hongqiling region, from west to east, along the southern margin of the Central Asian Orogenic Belt (CAOB) (e.g., Qin et al., 2011; Song et al., 2013, 2021; Wei et al., 2013). These discoveries indicate that orogenic belts have economic metallogenetic potential to host magmatic sulfide deposits. Nevertheless, occurrences of Ni-Cu sulfide deposits are rare in most of the orogenic belts worldwide throughout Earth's history (Song et al., 2018 and references therein). Basaltic magmatism with related mafic–ultramafic intrusions could be produced in different periods throughout the tectonic evolution of an orogenic belt, such as in subduction, collision or post-collision stages. The optimal period for extensive basaltic magmatism generating Ni-Cu sulfide mineralization during the development of orogenic belts is poorly known.

Among orogenic belts with sulfide deposits, the E-W-trending and ~600 km-long Huangshan-Jingerquan belt in the Tianshan Orogenic Belt is recognized as one of the largest Ni-Cu metallogenic belts worldwide. It is located at the southwestern margin of the Central Asian

* Corresponding authors at: Key Laboratory of Marine Hazards Forecasting, Ministry of Natural Resources (MNR), College of Oceanography, Hohai University, Nanjing 210098, China (Wei Xie).
E-mail addresses: weixie@hhu.edu.cn (W. Xie), chenliemeng@vip.gyig.ac.cn (L.-M. Chen).

https://doi.org/10.1016/j.oregeorev.2022.104837
Received 6 January 2022; Received in revised form 8 March 2022; Accepted 8 March 2022
Available online 11 March 2022

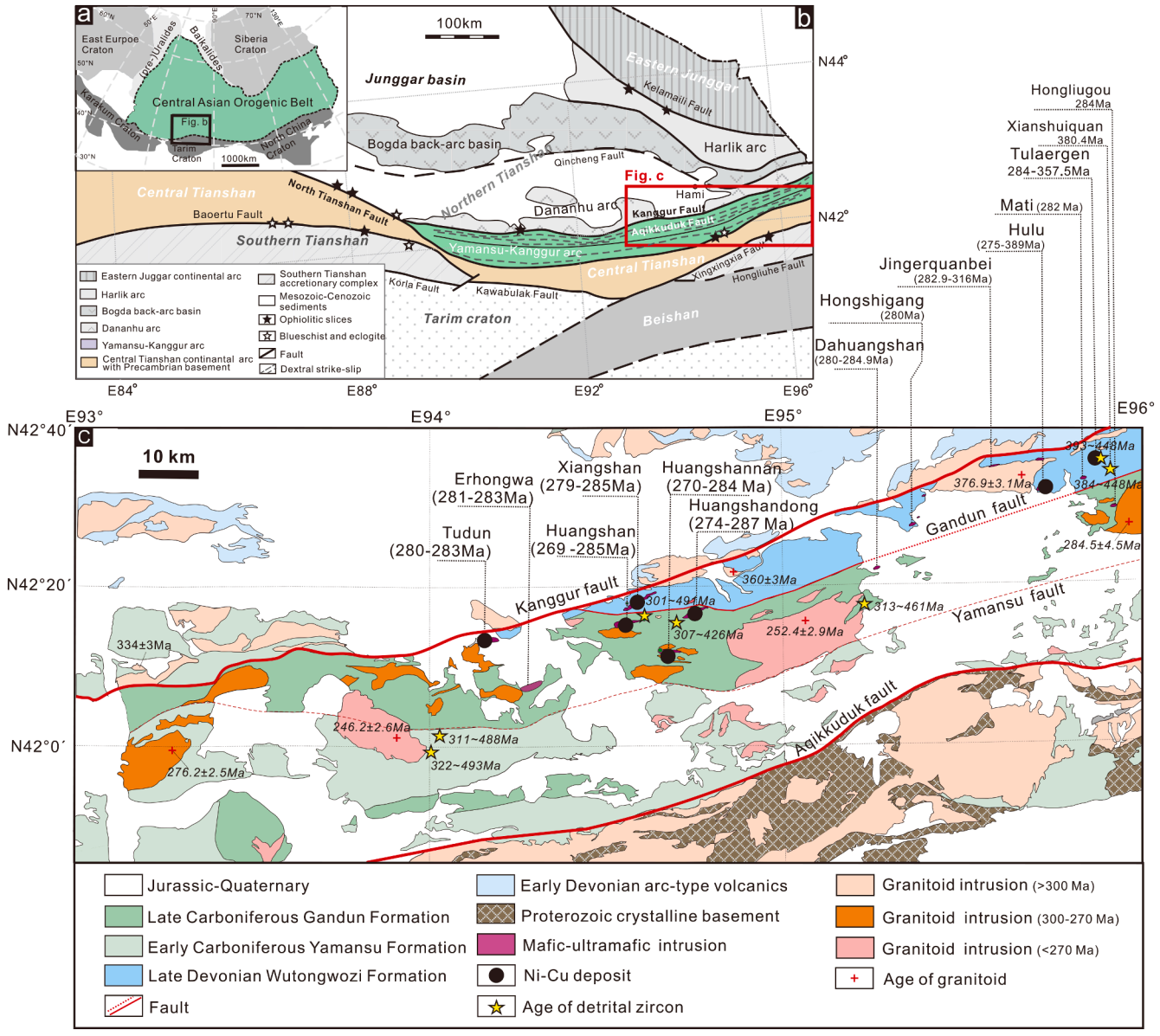

Fig. 1. a) Tectonic outline of the Central Asian Orogenic Belt and surrounding regions (after Şengör et al., 1993). b) Tectonic map of the Eastern Tianshan (modified after Xiao et al., 2004; Han and Zhao, 2018; Wang et al., 2018). c) Simplified geological map of the Kanggur-Yamansu arc, the Huangshan-Jingerquan Ni-Cu metallogenic belt is located to the north of the Yamansu fault (after Song et al., 2021).

Orogenic Belt, which is the largest Phanerozoic accretionary orogeny in the world (e.g., Şengör et al., 1993; Xiao et al., 2015). So far, seven sulfide deposits and > 10 potentially economic sulfide mineralization have been discovered in the Huangshan-Jingerquan belt. They contain more than one million tonnes of Ni metal reserves with 0.3 ~ 0.5% average Ni grades, which is ~30% of the total Ni metal reserves of sulfide deposits in orogenic belts of China (e.g., Zhou et al., 2004; Deng et al., 2014; Mao et al., 2016, 2018; Zhao et al., 2018b; Song et al., 2021). According to the latest geochronological study by Song et al. (2021), the mafic–ultramafic intrusions in the Huangshan-Jingerquan belt were regarded as the result of prolonged basaltic magmatism from 380 Ma to 270 Ma (late Devonian to early Permian; Zhou et al., 2004; San et al., 2010; Qin et al., 2011; Zhao et al., 2018b), whereas basaltic magmatism associated with Ni-Cu sulfide mineralization is very short-lived, ranging from 285 to 280 Ma (early Permian; Song et al., 2013; Deng et al., 2014; Zhao et al., 2015; Mao et al., 2016, 2018). The prolonged magmatic duration time of ~110 million years strikingly covered the subduction, collision and post-collision stages of the Tianshan Orogenic Belt (Xiao et al., 2004; Song et al., 2013; Han and Zhao, 2018; Xie et al., 2022). However, the tectonic stage to which the short-lived, sulfide mineralization-related basaltic magmatism belongs to remains poorly constrained.

Zircon U and Th concentrations are collected as part of U–Pb age determination and provide a wealth of information that is underutilized in understanding magmatic processes. According to zircon Th/U ratios are dominantly controlled by the silica content of the host melt and crystallization temperatures (Kirkland et al., 2015), McKay et al. (2018) suggests that zircon Th/U ratios record distinct magmatic conditions and may be correlated with tectonic environments (continental extension vs. compression) by studying felsic magmatic zircons and detrital zircons from the North American Cordillera. Extensional magmas (e.g., bimodal magmatism) is likely a result of hotter magmas (700 to > 1000 °C), increased fractionation, and more primitive mafic melts. Such extensional magmatism seems to be favorable for high Th/U zircon crystallization. Whereas active-margin magmatism during times of convergence, collision, and terrane accretion likely products felsic and

low temperature (~500° to 800 °C) magmas that favor low variability and decreased Th/U values. To test the utility of zircon Th/U ratios, they further evaluated U–Pb ages and Th/U ratios from southern Gondwanan zircons. The results reliably suggest that advancing extensional magmatism was associated with the unzipping of the Gondwanan margin from Australia to South America from ~340–250 Ma (Carboniferous to Triassic). Thus, in this contribution, the published Th/U ratios of zircons with U–Pb ages from the Huangshan-Jingerquan belt in the Eastern Tianshan, including magmatic zircons from mafic and felsic rocks and detrital zircons from sedimentary rocks, are revisited and integrated to address the optimal tectonic setting for these Permian sulfide deposits and mineralization.

2. Regional geological background

2.1. General geology of the Huangshan-Jingerquan Ni-Cu metallogenic belt

The Tianshan Orogenic Belt at the southwestern margin of the CAOB is subdivided into Western Tianshan and Eastern Tianshan roughly along longitude ~89°E in China. Eastern Tianshan is separated from the Eastern Junggar terrane to the north by the Kelamaili Suture and from the Tarim craton and Beishan belt to the south by the Kawabulak-Xingxingxia Fault (Fig. 1). It is divided into the North Tianshan arc system, the Central Tianshan continental arc, and the South Tianshan belt from north to south by the Kanggur Fault and the Xingxingxia Fault, respectively (e.g., Xiao et al., 2004; Xie et al., 2022).

The North Tianshan arc system is predominantly occupied by Paleozoic sedimentary-volcanic strata and magmatic intrusions. It is subdivided into the Harlik arc, the Bogda back-arc, the Dananhu arc from the north to the south separated by the Kanggur Fault (Fig. 1b; Xiao et al. 2004; Xie et al., 2016, 2022; Han and Zhao, 2018). Xiao et al. (2004) proposed that the Harlik-Dananhu arc was likely formed in early Ordovician and a back-arc basin (the Bogda basin) developed in early Carboniferous. The Central Tianshan arc is considered as a continental arc built on a Precambrian basement which is overlay by the Paleozoic volcanic-sedimentary strata at the southernmost margin of CAOB (Xiao et al., 2004; Charvet et al., 2007). The Kanggur-Yamansu arc is a forearc of the northern Central Tianshan continental arc due to southward subduction of the North Tianshan Ocean until the late Carboniferous (Fig. 1b; Du et al., 2018; Zhao et al., 2018a; Xie et al., 2022 and references therein).

The Kanggur-Yamansu arc is further subdivided into the Yamansu volcanic arc and Kanggur accretionary wedge on the two sides of the Yamansu Fault (Fig. 1c; Chen et al., 2019). The Kanggur accretionary wedge is dominantly composed of late Devonian (the Wutongwozi Formation) to late Carboniferous (the Gandun Formation) metasedimentary rock packages (Deng et al., 2021; Song et al., 2021). In contrast, the Yamansu volcanic arc primarily comprises Carboniferous volcanic-sedimentary sequences (Xie et al., 2022). In addition, the Main Tianshan Shear Zone acted on the Kanggur-Yamansu arc and resulted in extensive deformation between the Kanggur and Yamansu faults (Fig. 1c, Wang et al., 2014). Based on $^{40}Ar/^{39}Ar$ dating of micas- and amphibole-related materials, the deformation of the large-scale ductile shear zones initiated as early as ~ 300 Ma and extended to 230 Ma (Shu et al., 1999; Chen et al., 2005; Wang et al., 2008). The Huangshan-Jingerquan Ni-Cu metallogenic belt in the Eastern Tianshan is located northern of the Kanggur-Yamansu arc (Fig. 1c; Chen et al., 2019; Xie et al., 2022).

2.2. Mafic-ultramafic intrusions in the Huangshan-Jingerquan belt

The Huangshan-Jingerquan belt consists of a series of economic Ni-Cu sulfide deposits (Fig. 1). Among them, four large deposits (Huangshan, Huangshandong, Huangshannan and Tulaergen) and three medium-small deposits (Hulu, Xiangshan, and Tudun) have been identified (Deng et al., 2014, 2017; Zhao et al., 2015, 2018b; Mao et al., 2016, 2018; Song et al., 2021). Furthermore, the recent discoveries of Ni-Cu sulfide mineralization in more than ten intrusions (e.g., Erhongwa, Mati, Dahuagnshan) display great mineral exploration potential. These intrusions containing sulfide deposits and mineralization are generally comprised of lherzolite, websterite and harzburgite as the ultramafic facies and (olivine) gabbro, gabbronorite, norite and diorite as the mafic facies. The mafic and ultramafic rocks commonly contain 5–15 vol% hornblende and biotite. Sharp contacts among the mafic and ultramafic facies cannot be attributed to magma differentiation but reflect intermittent emplacement of multiple pulses of magma. Most lenticular Ni-Cu sulfide ore bodies and mineralization commonly occur at the bottom or middle of the ultramafic facies.

In addition, the mafic–ultramafic intrusions emplaced in the Gandun and Wutongwozi formations have distinct lithology and geometry features. The complexes emplaced in the Gandun Formation have large scales, teardrop, rhombic or oval outlines at the surface and funnel-shaped vertical cross sections, whereas the ultramafic facies of the complexes emplaced in the Wutongwozi Formation are commonly steep dikes or chains of small pods, although the mafic rocks may construct larger-scale intrusions (Lightfoot and Evans-Lamswood, 2015; Song et al., 2021).

2.3. Description of the studied samples

To reveal Th/U ratios of zircons with U–Pb ages along the Huangshan-Jingerquan belt, forty-four mafic rocks (SiO_2 < 55 wt%), seven felsic rocks (SiO_2 > 65 wt%) and nine sedimentary rocks with zircon U–Pb ages were collected in this study (Appendix). The forty-four mafic rocks contain thirty-two samples analyzed by secondary ion mass spectrometry (SIMS) analyses and twelve samples analyzed by laser ablation inductively coupled plasma–mass spectrometry (LA-ICP–MS). All felsic rocks and sedimentary rocks were analyzed by LA- ICP–MS. Among these samples, eleven mafic samples analyzed by SIMS, two mafic samples and five sedimentary rocks analyzed by LA-ICP–MS belong to our dataset that were published in Song et al. (2021) and Deng et al. (2021). These data are combined together to discuss distinguishingly from those of other literatures below. In addition, twenty-seven mafic and felsic rocks (nine by SIMS, eighteen by LA-ICP–MS) from the Tarim large igneous province were collected for comparison here (Appendix).

From the dating samples above, there are > 700 magmatic zircons of mafic rocks, > 100 magmatic zircons of felsic rocks, and ~ 700 detrital zircons from sedimentary rocks along the Huangshan-Jingerquan belt. The magmatic zircons display apparent $^{206}Pb/^{238}U$ ages ranging from 241 Ma to 394 Ma with scattered Th/U ratios (0.01 – 9.67), whereas the detrital zircons have apparent $^{206}Pb/^{238}U$ ages ranging from 301 Ma to 493 Ma with relatively restricted Th/U ratios from 0.01 to 2.56. In the Tarim large igneous province, there are > 400 magmatic zircons from mafic and felsic rocks. These magmatic zircons show apparent $^{206}Pb/^{238}U$ ages of 242 – 442 Ma (most are 260 – 300 Ma) and relatively limited Th/U ratios (most are 0.1 – 1.5).

3. Analytical method and results for zircon in-situ trace elements

3.1. Analytical method

Sixty-one magmatic zircons of two mafic rocks (*HSDD-01 gabbronorite and HSDD-02 lherzolite; mean U-Pb age with ~ 280 Ma*) from the Huangshandong intrusion, eighteen magmatic zircons of one gabbro sample (*H-4H; mean U-Pb age with ~ 389 Ma*) from the Hulu intrusion and four hundred and fifty-six detrital zircon grains from five sedimentary rocks (*DP1D-3, PD1-A, DP2D-1, TPD-8a and 1501D-1*) were selected for in-situ trace elements analyses here.

Zircon in-situ trace elements were measured by LA-ICP–MS at the *In*

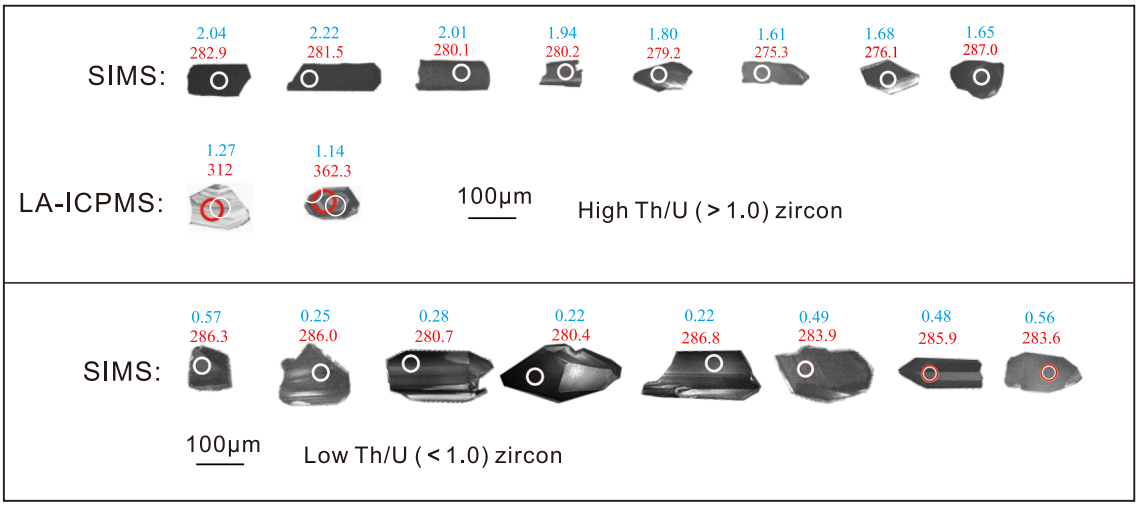

Fig. 2. CL images of representative zircons from Song et al. (2021) and Deng et al. (2021) are revisited, showing the high Th/U (>1.0) zircons have similar texture but smaller in grain size to low Th/U (<1.0) zircons. Red numbers are apparent $^{206}Pb/^{238}U$ ages and blue ones are Th/U ratios.

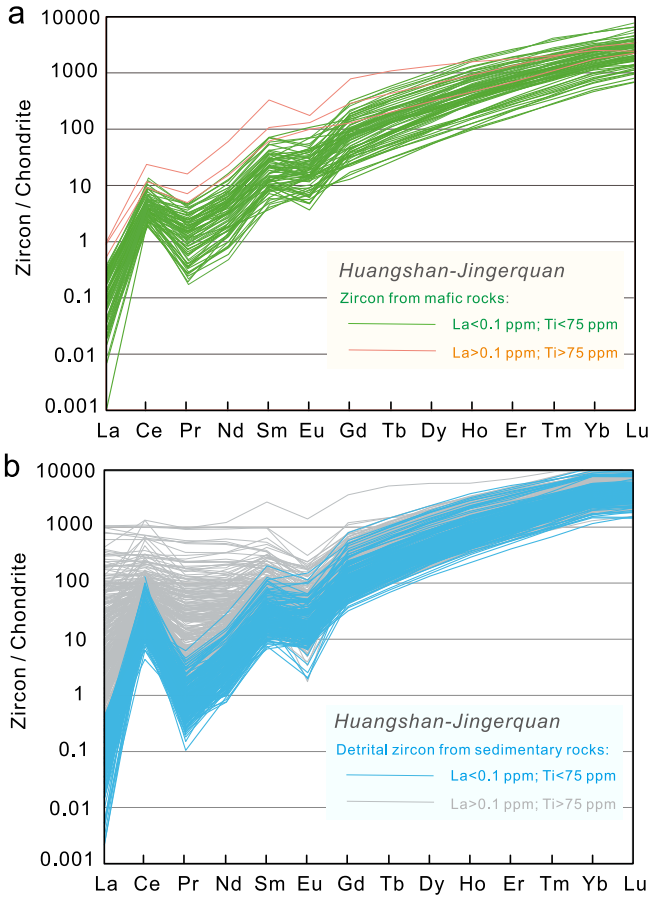

Fig. 3. Chondrite-normalized rare earth element patterns for (a) the magmatic zircons from mafic rocks and (b) detrital zircons from sedimentary rocks in the Huangshan-Jingerquan belt (chondrite data are from Sun and McDonough, 1989).

situ Mineral Geochemistry Lab, Ore deposit and Exploration Centre (ODEC), Hefei University of Technology, China. The analyses were carried out on an Agilent 7900 Quadrupole ICP–MS coupled to a Photon Machines Analyte HE 193-nm ArF Excimer Laser Ablation system equipped. Standard materials 91,500 and NIST 610 were used as external calibrations for the trace element content calculations, respectively. Zircon GJ-1 or Plešovice were analyzed between every 10 unknown samples for quality control. Each block of 8 unknowns was bracketed by analyses of standards. Each analysis began with a 20 s blank followed by a further 40 s analysis time after the laser was switched on. A laser beam of 30 μm in diameter was adopted at a repetition rate of 7 Hz and an energy density of 2.5 J/cm^2 (Ning et al., 2017; Wang et al., 2017). The off-line data processing was performed using a program called ICPMSDataCal (Liu et al., 2008). Trace element compositions of silicate minerals were calibrated against multiple-references materials without applying internal standardization. The sum of all element concentrations expressed as oxide (according to their oxidation states present in the silicate) are considered to be 100% m/m.

3.2. Results

Magmatic zircons from the Huangshandong and Hulu intrusions characteristically occur as irregular–subhedral crystals with coarse oscillatory zoning in cathodoluminescence (CL) images (Fig. 2), suggesting that they are typical zircons from gabbroic rocks that crystallized from fractionated interstitial melt late in the consolidation history of a cumulate (e.g., Scoates and Friedman, 2008). Their CL images and U–Pb ages were published in Song et al. (2021) and Zhao et al. (2018b). The in-situ zircon trace element data are listed in Appendix. Most zircons contain very low La (≤0.1 ppm) and Ti (up to 12.1 ppm) contents except three zircons (La 0.12 to 0.22 ppm) from HSDD-02. The normalized pattern is characterized by a steeply rising slope from light rare earth elements (LREEs) to heavy rare earth elements (HREEs) (Fig. 3a) with positive Ce anomalies (δCe [chondrite normalized $Ce/\sqrt{La \times Pr}$] = 2.7 to 32) and negative to positive Eu anomalies (δEu [chondrite normalized $Eu/\sqrt{Sm \times Gd}$] = 0.12 to 1.35, most < 1.0).

Most detrital zircons from the sedimentary rocks show euhedral–subhedral crystals with fine to coarse oscillatory zoning in CL images. The CL images and U–Pb ages of these detrital zircons were published in Deng et al. (2021). The in-situ zircon trace element data are listed in Appendix. About one hundred eighty detrital zircons contain very low La (≤0.1 ppm) and Ti (≤75 ppm) contents. They show relative LREE depletion and HREE enrichment (Fig. 3b) with positive Ce anomalies (δCe > 5) and negative Eu anomalies (δEu = 0.05 to 0.79).

4. Zircon filtration

McKay et al. (2018) discussed zircon Th/U ratios could record distinct magmatic conditions that are correlated with tectonic

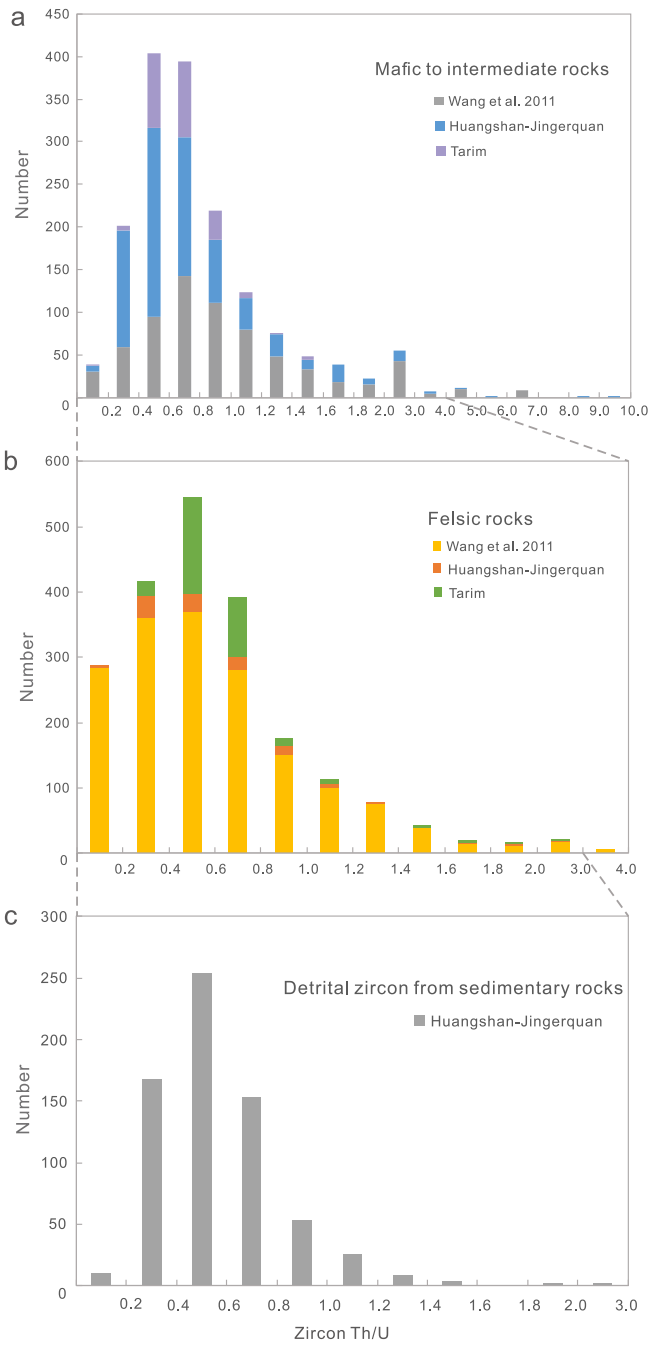

Fig. 4. Histogram of zircon Th/U ratios with intervals of 0.2 in (a) mafic to intermediate rocks, (b) felsic rocks and (c) sedimentary rocks from the Huangshan-Jingerquan belt. zircons from the Tarim large igneous province and Wang et al. (2011) are cited for comparison.

environments (continental extension vs. compression). This means that zircons should have formed from magmatic systems and that Th/U ratios should be unaffected by other conditions (e.g., metamorphism, alteration, inclusion and metamictization). To minimize the effect of these conditions, zircon filtration is necessary here.

First of all, a common observation is that most metamorphic zircons have Th/U ratios < 0.1, except in high-temperature and ultrahigh-temperature (UHT) metamorphic rocks, where the ratios are frequently > 0.1 (e.g., Rubatto, 2017; Yakymchuk et al., 2018 and references therein). The large-scale ductile shear zones along the Huangshan-Jingerquan belt are characterized by intensive deformation and very low-grade metamorphism without high-temperature and ultrahigh-temperature (UHT) metamorphic rocks (e.g., Branquet et al., 2012; Wang et al., 2014). Hence, the metamorphic zircons along the Huangshan-Jingerquan belt should have low Th/U ratios < 0.1. In addition, altered zircon or hydrothermal zircon is common in shear zones where the interaction of aqueous fluids with rocks is generally promoted. Alteration is often, but not necessarily, aided by prior metamictization, as damaged zircon domains are particularly prone to alteration by interaction with fluids. Consequently, altered zircon always displays dark CL rims with low Th/U < 0.1 (Kirkland et al., 2009; Rubatto, 2017). Therefore, we suggest that the > 0.1 Th/U zircons along the Huangshan-Jingerquan belt are magmatic in origin here and filter out thirteen zircons with Th/U < 0.1 that are potentially metamorphic and altered. In contrast, all zircons we collected from the Tarim large igneous province have ≥ 0.1 Th/U. Furthermore, the magmatic zircons from both the Huangshan-Jingerquan belt and the Tarim large igneous province with Th/U > 0.1 fall within the Th/U ranges of 0.1 – 9.0 for the mafic to intermediate rocks and 0.1 – 4.0 for the felsic rocks reported by Wang et al. (2011) (Fig. 4a, b). Detrital zircons from the Huangshan-Jingerquan belt favor Th/U ratios of 0.13 – 1.9, inferring that their source rocks might be magmatic rocks (Fig. 4c).

Secondly, a quantitative geochemical definition of "clean zircon" (inclusion- and crack-free zircon, which faithfully records the true magmatogenic zircon composition) forms the basis for discussion below. The inclusions within zircons contain enriched Th, Ti and LREEs, such as apatite, titanite or monazite, and promote anomalous Th/U ratios (Zou et al., 2019; Burnham, 2020). The analyzed spots are generally 10–20 μm spot size and < 2 μm ablation depth by SIMS analyses (Bowring et al., 2006; Li et al., 2015). Such a shallow ablation depth and small spot size could keep the analyzed spots off from the potential inclusions and cracks under clear CL images (Fig. 2). Additionally, the zircon SIMS data with > 0.1 Th/U we collected (our and literature data) have low common ^{206}Pb (<5%) except six spots that we would filter out later (Fig. 5a). This further suggests that these data are unaffected by inclusions or cracks in zircons. Thus, we think that the zircon data from the SIMS analyses could represent the original zircon composition. However, the LA-ICP–MS analyzed spots are generally 30–60 μm spot size and 20–30 μm ablation depth (Bowring et al., 2006; Li et al., 2015), which are potentially compromised by inclusions or cracks. Here, we select "clean zircon" with quantitative geochemical standards of zircon La ≤ 0.1 ppm and Ti ≤ 75 ppm suggested by previous studies (e.g., Hoskin and Schaltegger, 2003; Zou et al., 2019). Therefore, most magmatic zircons and approximately 180 detrital zircons from our LA-ICP–MS data are chosen for discussion below. The selected zircons have very low total Pb (<200 ppm) with irregular–subhedral shapes and coarse oscillatory zoning (Fig. 2). In addition, the literature LA-ICP–MS data have low total Pb (<500 ppm) without two spots, which we would also filter out later (Fig. 5b). We suggest that these literature LA-ICP–MS data could also represent the original zircon composition.

Finally, high U and Th concentrations of most grains lead to intensive metamictization by radiation damage. Radiation damage of high U and Th zircons may "soften" the microstructure of the zircon lattice, leading to the re-equilibration of U-Th-Pb isotopic systems of the zircon (Utsunomiya et al., 2007; Gao et al., 2014). In general, the U–Pb ages of magmatic zircons with low U contents (<1000 ppm) are relatively concentrated; however, high-U zircons (generally > 3000 ppm) often yield apparently scattered and older U–Pb ages (e.g., Williams and Hergt, 2000; White and Ireland, 2012). Similarly, high Th (>5000 ppm) also yields apparently scattered and older U–Pb ages. As shown in Fig. 6, the Th/U ratios of zircon show an obvious upward trend when the U and Th contents of zircon are > 3000 ppm and > 5000 ppm, respectively. This infers that the Th/U ratios of zircons might be influenced by the "high U(Th) effect". Hence, we also filter out zircons with high U (>3000 ppm) and Th (>5000 ppm) contents for discussion below.

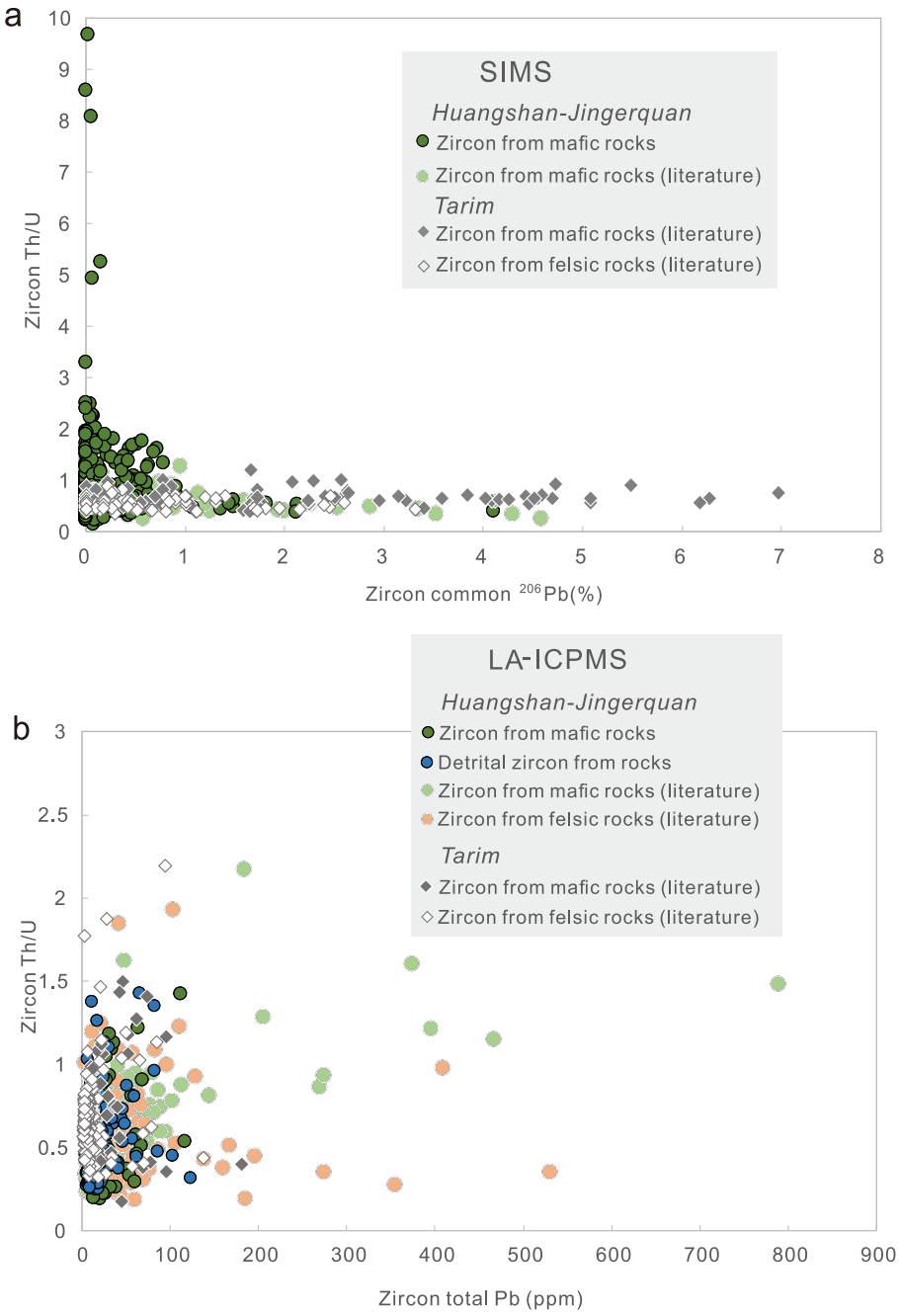

Fig. 5. (a) Plot of zircon Th/U versus common ^{206}Pb for the SIMS analyzed data. (b) Plot of zircon Th/U versus total Pb for the LA-ICP–MS analyzed data.

5. Discussion

5.1. Zircon Th/U ratios in the Huangshan-Jingerquan belt

The partition coefficient of U between zircon and melt (D_U) is approximately ten times larger than that of Th (D_{Th}) in felsic rocks, whereas D_U is about three times larger than D_{Th} in mafic to intermediate rocks (Wang et al., 2011). Consequently, zircon Th/U generally increases with decreasing SiO_2 content, such that zircon from gabbroic rocks has Th/U ratios largely between 0.8 and 1.2, while zircon Th/U from granitic rocks has distinctly lower ratios between 0.5 and 0.80 (Kirkland et al., 2015). Our collected samples display no relationship between Th/U ratios and whole-rock SiO_2 content (Fig. 7; Appendix). The natural samples with 35 ~ 55 wt% SiO_2 show lower Th/U ratios (0.3 – 1.0 in average value) than those of Kirkland et al. (2015), except two samples (1.4 – 1.8 in average value) with ~ 40 wt% SiO_2. However, zircons with high Th/U ratios (1.0 – 2.5) prefer to appear in mafic rocks, although the felsic rocks from the Huangshan-Jingerquan belt also contain some high Th/U zircons (Fig. 7). It is consistent with CL imageswhich show the high Th/U (>1.0) zircons have similar magmatic texture but smaller in grain size to low Th/U (<1.0) zircons (Fig. 2). Additionally, Th-bearing minerals (e.g., monazite, allanite) are usually co-crystallized with zircons in felsic or granitic melts which can result in generation of low Th/U zircons by relative competition. Even in some more silica-rich melts, melt polymerization and other Th or U-bearing minerals (e.g., xenotime or coffinite) can also control the zircon Th/U

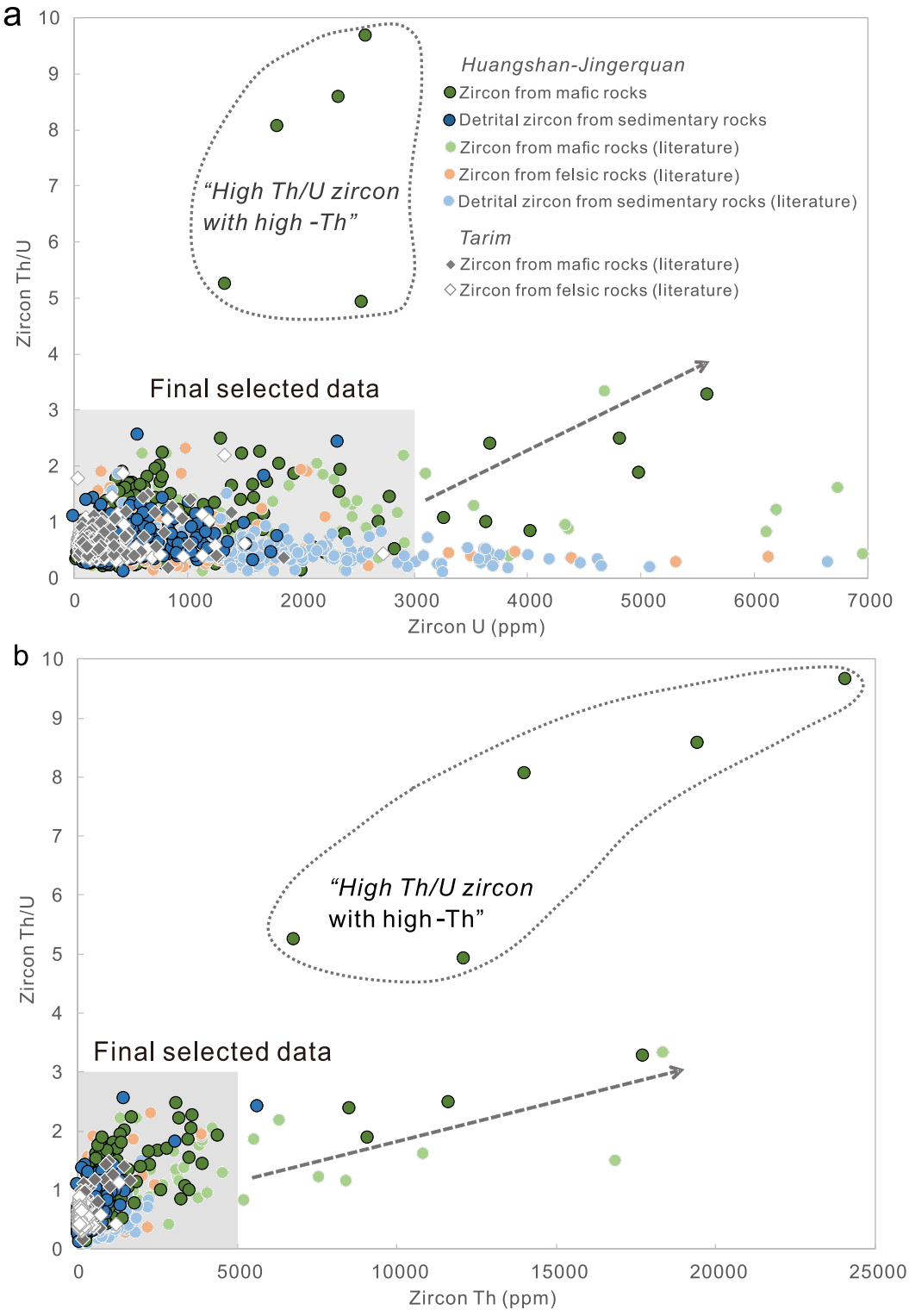

Fig. 6. (a, b) Plots of zircon Th/U versus U and Th concentrations. Data within the shadow field are the final selected data to discuss zircon Th/U ratios related to the tectonic stress regime.

ratios, but these seem to have a lesser influence (Miles et al., 2013; Kirkland et al., 2015). Whereas these minerals are generally absence in mafic magma. Thus, we consider that high zircon Th/U are preferably linked to low silica content (SiO_2 < 50 wt%) of the host melt (Kirkland et al., 2015). While a Th/U distinction can be made between the mafic and felsic end-members based on composition alone, zircon Th/U from intermediate compositions, would be affected by additional factors, such as redox conditions, where oxygen fugacity (f_{O2}) and zircon Th/U are inversely related (Burnham and Berry, 2012). Ce anomalies (δCe) in zircon are redox sensitive because cerium always occurs as Ce^{4+} in an oxidized magma and Ce^{4+} has an ionic radius of 0.97 Å, close to Lu, similar to HREEs (e.g., Hoskin and Schaltegger, 2003). Both magmatic zircons from mafic rocks and detrital zircons from sedimentary rocks in the Huangshan-Jingerquan belt show no relationship between zircon

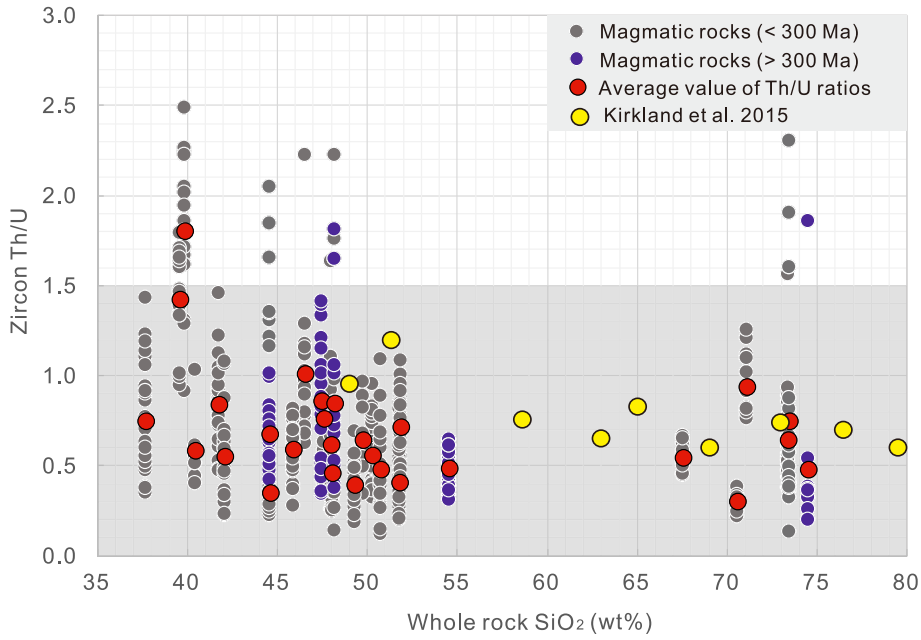

Fig. 7. Plot of zircon Th/U versus whole rock SiO_2 for magmatic rocks from the Huangshan-Jingerquan belt. Red spots represent the average of Th/U ratios for each sample. Data from Kirkland et al. (2015) are cited for comparison

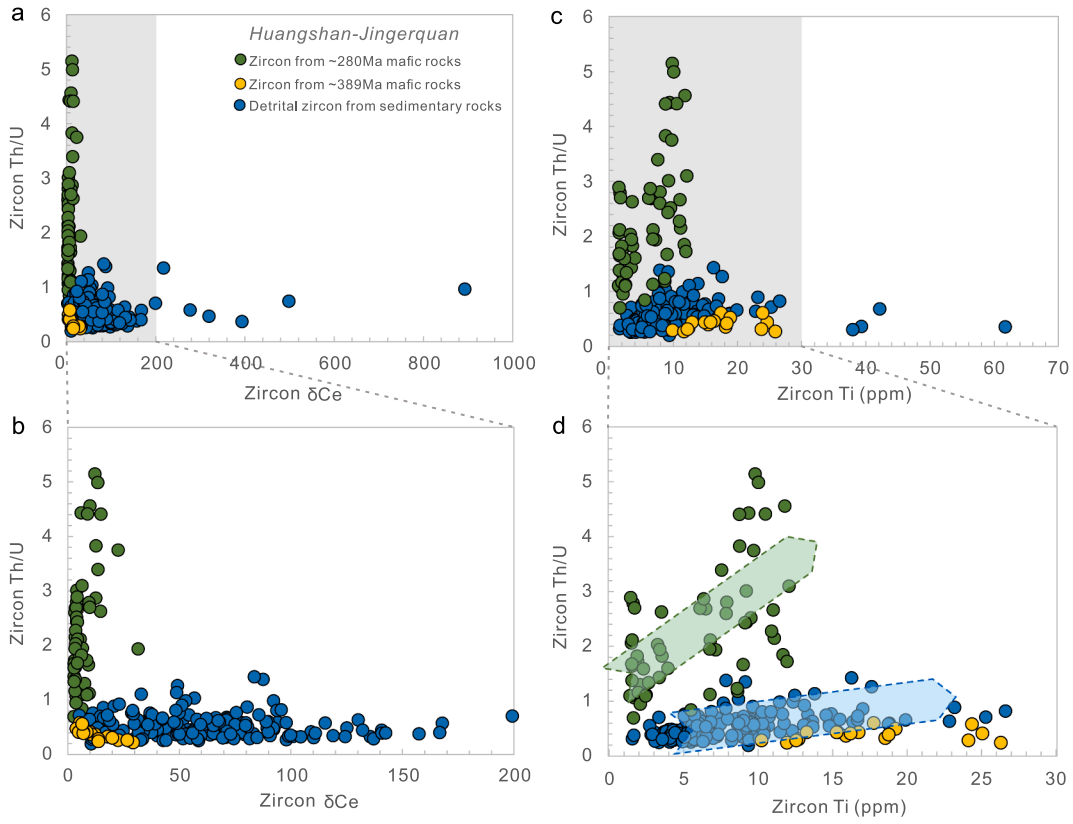

Fig. 8. Plots of zircon Th/U versus δCe (a, b) and Ti (c, d) concentrations.

Th/U and δCe (Fig. 8a, b), inferring that oxygen fugacity (f_{O2}) can be ignored here.

Furthermore, a temperature effect (i.e., crystallization temperature) likely controls zircon Th/U ratios together. Higher crystallization temperatures in the mafic to intermediate melts relative to felsic rocks cause an expansion of the crystal lattice and favor the substitution of elements with larger ionic radii (e.g., U relative Zr and Th relative to U). However, Kirkland et al. (2015) discussed that there is a trend toward lower zircon Th/U with increasing temperature under equilibrium conditions which can be attributed to lattice strain from experimental partition coefficient studies. Whereas within a nonequilibrium and fractionating magma, temperatures yield the relationship of lower zircon Th/U in cooler melts.

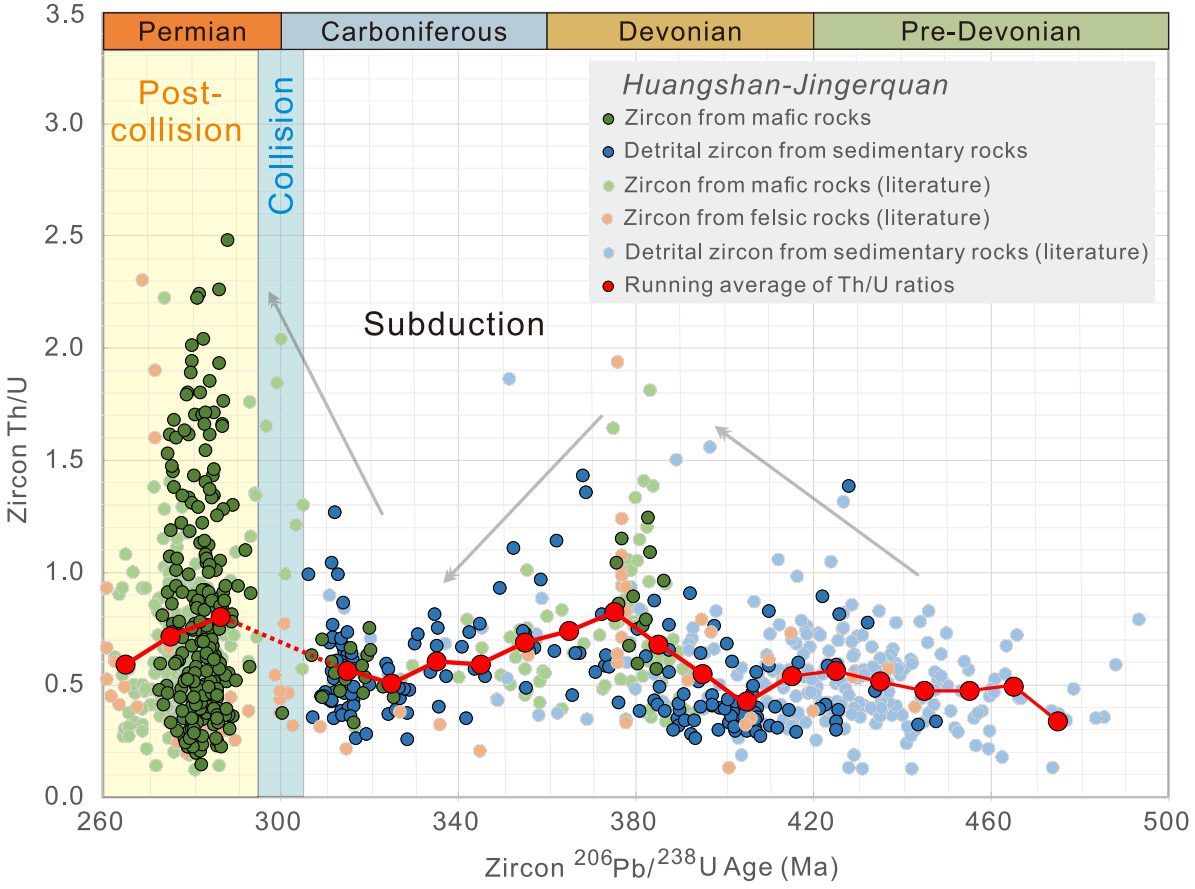

Fig. 9. Zircon Th/U versus apparent $^{206}Pb/^{238}U$ ages from the Huangshan-Jingerquan belt. Running average is calculated with increments of 10 million years. The average values between 290 and 310 Ma have not given here due to a few data.

This is due to zircon growth under nonequilibrium conditions with greater incompatibility of Th relative to U and the removal and segregation of mineral precipitates (Kirkland et al., 2015). Actually, zircon as an accessory mineral always grow late within a compositionally fractioned and nonequilibrium melt pocket, especially in hotter mafic magma (mesostasis; Williams, 1978). Titanium in zircon is highly sensitive to temperature not only in felsic magma systems (e.g., Watson and Harrison, 2005; Watson et al., 2006) but also in mafic magma systems (e.g., Fu et al., 2008). Generally, Ti in zircon increases while temperature increases in magma systems, although other functions may affect Ti concentration, such as a_{TiO2} or a_{SiO2} (the activity of TiO_2 or SiO_2), variable pressure, deviations from Henry's Law, and subsolidus Ti exchange (e.g., Ferry and Watson, 2007; Fu et al., 2008). Detrital zircons from sedimentary rocks and magmatic zircons from mafic rocks in the Huangshan-Jingerquan belt display two independent positive correlations between zircon Th/U and Ti concentrations (Fig. 8c, d), indicating that zircon Th/U ratios in the Huangshan-Jingerquan belt are linked to crystallization temperatures under zircon growth with fractionating melts as well as the silica content of the host melt (e.g., Wang et al., 2011; Kirkland et al., 2015).

McKay et al. (2018) suggests that zircon Th/U may be correlated with end-member tectonic stress regimes (continental extension vs. compression) that correlate with distinct magmatic conditions by studying felsic magmatic zircons and detrital zircons from the North American Cordillera. They argued that magmatism coeval with extensional tectonism tends to produce zircon with a wider range of Th/U values, including significant populations of elevated Th/U zircon (>1.0) and very few zircons with Th/U < 0.25. Active-margin magmatism during times of convergence, collision, and terrane accretion is more conducive to producing low zircon Th/U (<1.0) with little geochemical variability. The relationship of high Th/U variability and elevated zircon Th/U associated with extensional magmas is likely a result of hotter magmas (700 to > 1000 °C), increased fractionation, and more primitive mafic melts (Kirkland et al., 2015), which is consistent with known compositional trends in extensional magmas. Low variability and decreased Th/U values for collisional and continental arc magmas may represent lower temperature conditions (500 to 800 °C), long-duration magmatic source rejuvenation, or silica-rich melts. McKay et al. (2018) also tested zircon Th/U ratios and tectonic settings in the South America, South Africa, Antarctica and Australia, indicating that the ratio could record the useful information of regional tectonic stress regimes. To reveal the tectonic evolution of the Huangshan-Jingerquan belt, zircon Th/U ratios with U–Pb ages from this belt will be discussed in detail below.

5.2. Tectonic implication

Recent geochronology and geochemistry studies have demonstrated that the Carboniferous calc-alkaline and tholeiite volcanics and I-type felsic intrusions in the Kanggur-Yamansu arc as a forearc system of the Central Tianshan continental arc resulted from southward subduction of the North Tianshan Ocean (e.g., Du et al., 2018; Zhao et al., 2018a; Xie et al., 2022 and references therein). Many studies consider that the Kanggur-Yamansu arc has transitioned into a post-collision extensional setting during the early Permian (e.g., Han and Zhao, 2018; Song et al., 2021 and references therein), based on extensive occurrences of the early Permian bimodal volcanic rocks (e.g., Chen et al., 2011) and A_2-type granitoids (e.g., Yuan et al., 2010) in the adjacent Harlik-Dananhu arc. Bimodal volcanic rocks are rare in the Kanggur-Yamansu arc, although bimodal intrusions were reported by Muhtar et al. (2020). A

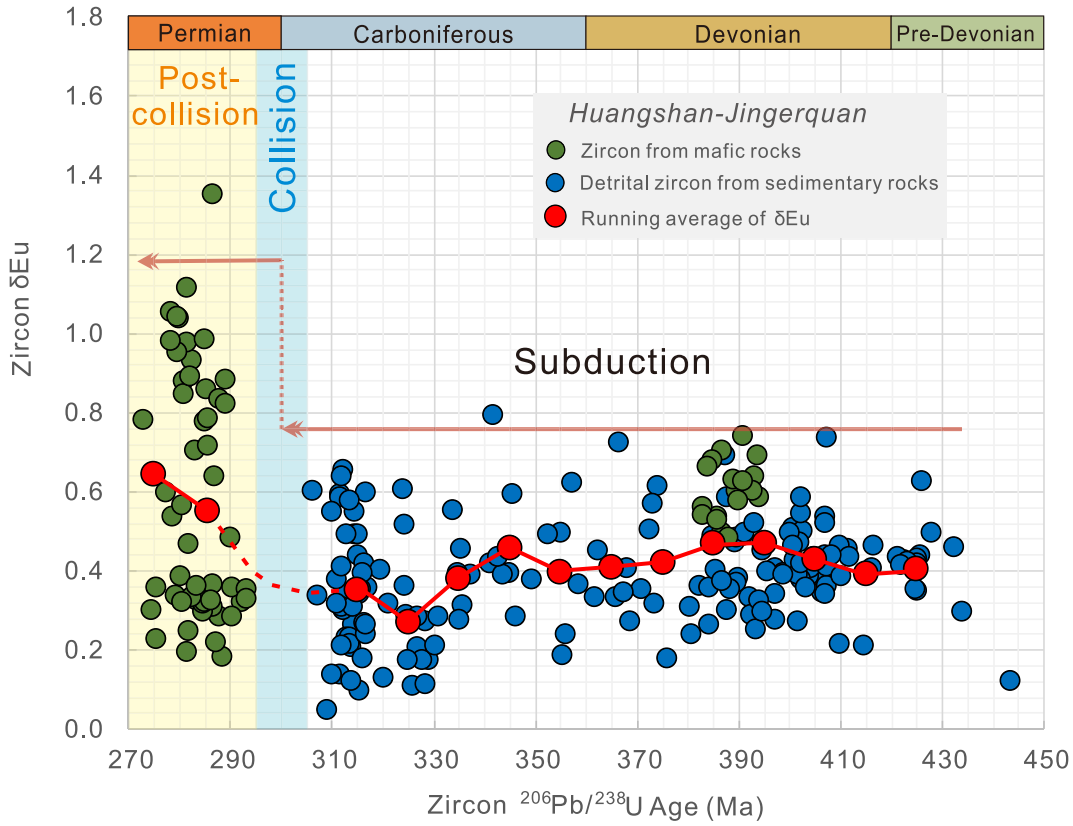

Fig. 10. Zircon δEu versus apparent $^{206}Pb/^{238}U$ ages from the Huangshan-Jingerquan belt. Running average is calculated with increments of 10 million years.

few early Permian A_2-type granites (284 – 292 Ma) were sparse in the western Kanggur-Yamansu arc, whereas some early Permian I-type granites (276 – 288 Ma) occurred in the eastern part of the region (e.g., Zhang et al., 2014; Du et al., 2018). Consequently, Zhang et al. (2014) suggested that the eastern Kanggur-Yamansu arc where the Huangshan-Jingerquan belt occurs, was in a compressional tectonic setting. In addition, some studies argued the Kanggur-Yamansu arc are still an advancing subduction (e.g., Xiao et al., 2004; Ao et al., 2010) or a *syn*-collisional setting (e.g., Deng et al., 2015). Others discussed that sulfide-mineralized/bearing ultramafic–mafic intrusions (~270 – 290 Ma; Zhou et al., 2004; Qin et al., 2011; Su et al., 2011) and early Permian A-type granites (~290 Ma; Pirajno et al., 2008; Liu et al., 2013) in the Kanggur-Yamansu arc were attributed to the Tarim mantle plume under the Permian Tarim large igneous province (~280 – 290 Ma; Xu et al., 2014). Therefore, the tectonic environment during the early Permian in the Huangshan-Jingerquan belt of the Kanggur-Yamansu arc remains debated.

Whole-rock trace elements and Sr-Nd isotopes of the mafic–ultramafic intrusions in the Huangshan-Jingerquan belt are distinct from those of the Permian Tarim large igneous province (e.g., Song et al., 2013, Deng et al., 2015). Magmatic zircons from the Huangshan-Jingerquan belt also have higher U (up to 7000 ppm) and Th (up to 18000 ppm) concentrations and Th/U ratios (0.01 to 2.5 after filtration) than those of the Permian Tarim large igneous province (U < 1900 ppm, Th < 1700 ppm, most Th/U < 1.5; Fig. 6). Additionally, the Permian Tarim mantle plume could not account for the 300 – 380 Ma gabbros in the Huangshan-Jingerquan complexes. Thus, the prolonged basaltic magmatism along the Huangshan-Jingerquan belt was more likely associated with subduction-collision processes (Song et al., 2021).

The Huangshan-Jingerquan belt is dominantly composed of late Devonian to late Carboniferous volcanic-sedimentary sequences. Post-Carboniferous sequences are very rare. Subsequently, detrital zircons from the post-Carboniferous sequences have not been reported yet. Fortunately, abundant magmatic zircons from 260 ~ 300 Ma mafic to felsic intrusions are published (Song et al., 2021 and references therein). These data give us a valuable opportunity to address the optimal tectonic setting for these Permian sulfide deposits and mineralization. Detrital zircons from sedimentary rocks dominantly represent zircons from felsic products of crustal melts. As zircons grains in small size of mafic rocks, they are few in detrital zircons and usually suffer metamictization more easily and then possibly to filter out by our filtering method above. Nevertheless, Detrital zircons (>300 Ma) in the Huangshan-Jingerquan belt display synchronous changes very well with ages relative to magmatic zircons from the mafic and felsic rocks (Fig. 9). As shown in Fig. 9, most zircon Th/U ratios are < 1.0, and elevated (1.0 to 2.5) Th/U zircons are 360 ~ 390 Ma (late Devonian) or 270 ~ 300 Ma (early Permian) in age, indicating that the Huangshan-Jingerquan belt was an extensional environment during the two periods. This is consistent with the early Permian short-durational bimodal magmatism (Muhtar et al., 2020; Song et al., 2021), which could generate highly variable and elevated zircon Th/U (1.0 to > 3.5) suggested by McKay et al. (2018). Therefore, it argues against the Huangshan-Jingerquan belt was an advancing subduction or a *syn*-collisional setting during the early Permian. Th/U ratios (>1.0) at 360 ~ 390 Ma infer that the late Devonian might be another extensional tectonic stage (e.g., a retreating subduction setting) that has not yet been recognized in the region. As the Huangshan-Jingerquan belt is close to the Kanggur Fault, which represents the southernmost suture of the North Tianshan Ocean, low zircon Th/U (<1.0) ratios in the Carboniferous and pre-Devonian should be related to a compressional arc front setting (e.g., Chen et al., 2019; Xie et al., 2022) where lower temperature, long-lived, felsic magmas are more conducive to low Th/U (<1.0) zircon crystallization.

Tang et al. (2021) proposed zircon δEu as a new proxy to infer crustal thickness because it is positively correlated with crustal thickness, which can be explained by two processes favored during high-pressure

differentiation: (1) suppression of plagioclase and (2) endogenic oxidation of Eu^{2+} due to garnet fractionation. They further provided an empirical equation that calculates crustal thickness from zircon δEu by compiling zircon data from global intermediate to felsic rocks. Although mafic samples were not considered in their studies, zircon δEu from the mafic magma is also predominantly attributed to the two factors above. In Fig. 10, zircon δEu is roughly constant within low < 0.8 δEu from 450 to 310 Ma, although zircons from mafic rocks have a little higher δEu than those of detrital zircons. And then δEu elevated sharply to 1.2 (even one spot is up to 1.4) at 290 – 270 Ma. This indicates that the crust in the Huangshan-Jingerquan belt was thickened from the late Carboniferous to early Permian. Consequently, the Huangshan-Jingerquan belt was an extensional environment but with thicker crust in the early Permian than in the pre-Permian, suggesting that the belt was induced by the tectonic transition from a continental arc to a post-collisional environment due to collision between the Kanggur-Yamansu and Harlik-Dananhu arcs at ~ 300 Ma (e.g., Du et al., 2018; Han and Zhao, 2018; Muhtar et al., 2020; Xie et al., 2022). In addition, recent studies indicated that the regional strike-slip shearing along the Huangshan-Jingerquan belt began at ~ 300 Ma simultaneously with the collision (e.g., Shu et al., 1999; Chen et al., 2005; Wang et al., 2008, 2014). Considering the occurrences of the early Permian terrestrial sandstone and conglomerate relative to the Carboniferous shallow marine sedimentary (Wartes et al., 2002), the collective lines of evidence suggest that the Permian short-lived (<5 Ma) Ni-Cu sulfide deposits in the region were likely formed in a post-collision extensional setting. Based on petro-structural analysis and strain rate calculation, Branquet et al. (2012) proposed that regional strike-slip shearing created transtensive spaces for ascending of the basaltic magma and formation of magma chambers. Thus, the Huangshan and Huangshandong complexes have teardrop and rhombic shapes and the wall rocks have been tightly folded with long axis parallel to the foliation (Lightfoot and Evans-Lamswood, 2015; Song et al., 2021). It is noteworthy that a few of sulfide-mineralized mafic–ultramafic intrusions were formed during a subduction period along the southern margin of the CAOB, such as the Heishan intrusion (~357 Ma, Xie et al., 2012). However, these deposits are much smaller than those along the Huangshan-Jingerquan belt. Therefore, the most important period for the formation of Ni-Cu sulfide deposit in orogenic belts is the post-collision extensional stage.

6. Conclusions

Zircon Th/U ratios are an effective tracer to reveal the tectonic stress regimes (continental extension vs. compression). However, zircon filtration is necessary before using it to minimize the effect of amagmatic conditions (e.g., metamorphism, alteration, inclusion and metamictization). The Th/U ratios of a new zircon data compilation from the Huangshan-Jingerquan belt is likely linked to both the silica content of the magma and crystallization temperatures under zircon growth with fractionating melts after zircon filtration. High Th/U ratios (up to 2.5) during the early Permian indicate that the region was in an extensional environment at that time. Low zircon Th/U (<1.0) ratios in the Carboniferous and pre-Devonian are related to a compressional arc front setting. Combined with zircon δEu data, we finally suggest that the Permian short-lived (<5 Ma) Ni-Cu sulfide deposits in the region formed in a post-collision extensional setting that is likely the optimal condition for the formation of economic Ni-Cu sulfide deposit in orogenic belts.

Declaration of Competing Interest

The authors declare that they have no known competing financial interests or personal relationships that could have appeared to influence the work reported in this paper.

Acknowledgements

This study was financially supported by funds from the Key Special Project for Introduced Talents Team of Southern Marine Science and Engineering Guangdong Laboratory (Guangzhou) (GML2019ZD0202) and NSFC research grants (41630316, 41873031, U1803113). Hang-Qiang Xie at the Beijing SHRIMP Centre (National Science and Technology Infrastructure) and Fang-Yue Wang at Hefei University of Technology are thanked for help with technical assistance. The quality of this manuscript was greatly improved by the constructive comments from three anonymous reviewers, and the editor, Franco Pirajno.

Appendix A. Supplementary data

Supplementary data to this article can be found online at https://doi.org/10.1016/j.oregeorev.2022.104837.

References

Ao, S.J., Xiao, W.J., Han, C.M., Mao, Q.G., Zhang, J.E., 2010. Geochronology and geochemistry of Early Permian mafic-ultramafic complexes in the Beishan area, Xinjiang, NW China: Implications for late Paleozoic tectonic evolution of the southern Altaids. Gondwana Res. 18 (2-3), 466–478.

Bowring, S.A., Schoene, B., Crowley, J.L., Ramezani, J., Condon, D.J., 2006. High-precision U–Pb geochronology and the stratigraphic record: progress and promise. In: Olszewski, T.D. (Ed.), Geochronology, Emerging Opportunities. The Paleontological Society Special Publication, 12, pp. 25–46.

Branquet, Y., Gumiaux, C., Sizaret, S., Barbanson, L., Wang, B., Cluzel, D., Li, G.G., Delaunay, A., 2012. Synkinematic mafic/ultramafic sheeted intrusions: Emplacement mechanism and strain restoration of the Permian Huangshan Ni-Cu ore belt (Eastern Tianshan, NW China). J. Asian Earth Sci. 56, 240–257.

Burnham, A.D., Berry, A.J., 2012. An experimental study of trace element partitioning between zircon and melt as a function of oxygen fugacity. Geochim. Cosmochim. Acta 95, 196–212.

Burnham, A.D., 2020. Key concepts in interpreting the concentrations of the rare earth elements in zircon. Chem. Geol. 551, 1–8.

Charvet, J., Shu, L.S., Laurent-Charvet, S., 2007. Paleozoic structural and geodynamic evolution of eastern Tianshan (NW China): welding of the Tarim and Junggar plates. Episodes 30, 162–186.

Chen, W., Sun, S., Zhang, Y., Xiao, W.-J., Wang, Y.-T., Wang, Q.-L., Jiang, L.-F., Yang, J.-T., 2005. $^{40}Ar/^{39}Ar$ geochronology of the Qiugemingtashi-Huangshan ducile shear zone in East Tianshan, Xinjiang, NW China. Acta Geological Sinica 79, 790–804 (in Chinese with English abstract).

Chen, X., Shu, L., Santosh, M., 2011. Late Paleozoic post-collisional magmatism in the Eastern Tianshan Belt, Northwest China: new insights from geochemistry, geochronology and petrology of bimodal volcanic rocks. Lithos 127 (3-4), 581–598.

Chen, Z., Xiao, W., Windley, B.F., Schulmann, K., Mao, Q., Zhang, Z., Zhang, J., Deng, C., Song, S., 2019. Composition, provenance and tectonic setting of the Southern Kangurtag accretionary complex in the Eastern Tianshan, NW China: implications for the late Paleozoic evolution of the North Tianshan Ocean. Tectonics 38 (8), 2779–2802.

Deng, Y.F., Song, X.Y., Chen, L.M., Zhou, T.F., Pirajno, F., Yuan, F., Xie, W., Zhang, D.Y., 2014. Geochemistry of the Huangshandong Ni-Cu deposit in northwestern China: Implications for the formation of magmatic sulfide mineralization in orogenic belts. Ore Geol. Rev. 56, 181–198.

Deng, Y.F., Song, X.Y., Hollings, P., Zhou, T., Yuan, F., Chen, L.M., Zhang, D.Y., 2015. Role of asthenosphere and lithosphere in the genesis of the Early Permian Huangshan mafic-ultramafic intrusion in the Northern Tianshan, NW China. Lithos 227, 241–254.

Deng, Y.-F., Song, X.-Y., Hollings, P., Chen, L.-M., Zhou, T., Yuan, F., Xie, W., Zhang, D., Zhao, B., 2017. Lithological and geochemical constraints on the magma conduit systems of the Huangshan Ni-Cu sulfide deposit, NW China. Miner. Deposita 52 (6), 845–862.

Deng, Y., Song, X., Jie, W., Yuan, F., Zhao, Z., Wei, S., Zhu, J., Kang, J., Wang, K., Liang, Q., Chen, L., Yu, S., 2021. Determination of sedimentary ages of strata in the H uangshan-Jingerquan mineralization belt and its geological significance. Acta Geol. Sin. 95, 362–376 (in Chinese with English abstract).

Du, L., Long, X., Yuan, C., Zhang, Y., Huang, Z., Wang, X., Yang, Y., 2018. Mantle contribution and tectonic transition in the Aqishan-Yamansu Belt, Eastern Tianshan, NW China: Insights from geochronology and geochemistry of Early Carboniferous to Early Permian felsic intrusions. Lithos 304–307, 230–244.

Ferry, J.M., Watson, E.B., 2007. New thermodynamic models and revised calibrations for the Ti-in-zircon and Zr-in-rutile thermometers. Contrib. Miner. Petrol. 154 (4), 429–437.

Fu, B., Page, F.Z., Cavosie, A.J., Fournelle, J., Kita, N.T., Lackey, J.S., Wilde, S.A., Valley, J.W., 2008. Ti-in-zircon thermometry: applications and limitations. Contrib. Miner. Petrol. 156 (2), 197–215.

Gao, Y.-Y., Li, X.-H., Griffin, W.L., O'Reilly, S.Y., Wang, Y.-F., 2014. Screening criteria for reliable U-Pb geochronology and oxygen isotope analysis in uranium-rich zircons: A case study from the Suzhou A-type granites, SE China. Lithos 192–195, 180–191.

Han, Y., Zhao, G., 2018. Final amalgamation of the Tianshan and Junggar orogenic collage in the southwestern Central Asian Orogenic Belt: constraints on the closure of the Paleo-Asian Ocean. Earth-Science Review 186, 129–152.
Hoskin, P.W.O., 2003. The Composition of Zircon and Igneous and Metamorphic Petrogenesis. Rev. Mineral. Geochem. 53 (1), 27–62.
Kirkland, C.L., Whitehouse, M.J., Slagstad, T., 2009. Fluid-assisted zircon and monazite growth within a shear zone: a case study from Finnmark, Arctic Norway. Contrib. Miner. Petrol. 158 (5), 637–657.
Kirkland, C.L., Smithies, R.H., Taylor, R.J.M., Evans, N., Mcdonald, B., 2015. Zircon Th/U ratios in magmatic environs. Lithos 212–215, 397–414.
Li, X.H., Liu, X.M., Liu, Y.S., Su, L., Sun, W.D., Huang, H.Q., Yi, K., 2015. Accuracy of LA-ICPMS zircon U-Pb age determination: an inter-laboratory comparison. Sci. China Earth Sci. 58 (10), 1722–1730.
Lightfoot, P.C., Evans-Lamswood, D., 2015. Structural controls on the primary distribution of mafic-ultramafic intrusions containing Ni-Cu-Co-(PGE) sulfide mineralization in the roots of large igneous provinces. Ore Geol. Rev. 64, 354–386.
Liu, H.Q., Xu, Y.G., He, B., 2013. Implications from zircon-saturation temperatures and lithological assemblages for Early Permian thermal anomaly in northwest China. Lithos 182–183, 125–133.
Liu, Y., Hu, Z., Gao, S., Günther, D., Xu, J., Gao, C., Chen, H., 2008. In situ analysis of major and trace elements of anhydrous minerals by LA-ICP–MS without applying an internal standard. Chem. Geol. 257 (1-2), 34–43.
Liu, Y.G., Li, W.Y., Jia, Q.Z., Zhang, Z.W., Wang, Z.A., Zhang, Z.B., Zhang, J.W., Qian, B., 2018. The dynamic sulfide saturation process and a possible slab break-off model for the giant Xiarihamu magmatic nickel ore deposit in the East Kunlun Orogenic Belt, Northern Qinghai-Tibet Plateau, China. Econ. Geol. 113, 1383–1417.
Mao, Y.J., Qin, K.Z., Tang, D.M., Feng, H.Y., Xue, S.C., 2016. Crustal contamination and sulfide immiscibility history of the Permian Huangshannan magmatic Ni-Cu sulfide deposit, East Tianshan, NW China. J. Asian Earth Sci. 129, 22–37.
Mao, Y.J., Qin, K.Z., Tang, D.M., 2018. Revisiting the age and emplacement process of the huangshandong Ni-Cu deposit in the Central Asian Orogenic belt, northwestern China: implications for multiple magma extractions from a short-lived staging magma chamber. Lithos 320–321, 583–591.
McKay, M.P., Jackson, W.T., Hessler, A.M., 2018. Tectonic stress regime recorded by zircon Th/U. Gondwana Res. 57, 1–9.
Miles, A.J., Graham, C.M., Hawkesworth, C.J., Gillespie, M.R., Hinton, R.W., 2013. Evidence for distinct stages of magma history recorded by the compositions of accessory apatite and zircon. Contrib. Miner. Petrol. 166 (1), 1–19.
Muhtar, M.N., Wu, C.Z., Santosh, M., Lei, R.X., Gu, L.X., Wang, S.M., Gan, K., 2020. Late Paleozoic tectonic transition from subduction to post-collisional extension in Eastern Tianshan, Central Asian Orogenic Belt. Geol. Soc. Am. Bull. 132, 1756–1774.
Ning, S., Wang, F., Xue, W., Zhou, T., 2017. Geochemistry of the Baoshan pluton in the Tongling region of the Lower Yangtze River Belt. Geochimica 46, 397–412 (in Chinese with English abstract).
Qin, K.-z., Su, B.-x., Sakyi, P.A., Tang, D.-m., Li, X.-h., Sun, H., Xiao, Q.-h., Liu, P.-p., 2011. SIMS zircon U-Pb geochronology and Sr-Nd isotopes of Ni-Cu-bearing mafic-ultramafic intrusions in eastern Tianshan and Beishan in correlation with flood basalts in Tarim basin (NW China): constraints on a ca. 280 Ma mantle plume. Am. J. Sci. 311 (3), 237–260.
Pirajno, F., Mao, J., Zhang, Z., Zhang, Z., Chai, F., 2008. The association of mafic–ultramafic intrusions and A-type magmatism in the Tian Shan and Altay orogens, NW China: implications for geodynamic evolution and potential for the discovery of new ore deposits. J. Asian Earth Sci. 32 (2-4), 165–183.
Rubatto, D., 2017. Zircon: the metamorphic mineral. Rev. Mineral. Geochem. 83, 261–295.
San, J.Z., Qin, K.Z., Tang, Z.I., Tang, D.M., Su, B.X., Sun, H., Xiao, Q.H., Liu, P.P., 2010. Precise zircon U-Pb age dating of two mafic ultramafic complexes at Tulargen large Cu-Ni district and its geological implications. Acta Petropgica Sinica 26, 3027–3035 (in Chinese with English abstract).
Scoates, J.S., Friedman, R.M., 2008. Precise age of the platiniferous Merensky Reef, Bushveld Complex, South Africa, by the U-Pb zircon chemical abrasion ID-TIMS technique. Econ. Geol. 103 (3), 465–471.
Şengör, A.M.C., Natal'in, B.A., Burtman, V.S., 1993. Evolution of the Altaid tectonic collage and Palaeozoic crustal growth in Eurasia. Nature 364 (6435), 299–307.
Shu, L.S., Charvet, J., Guo, L.Z., Lu, H.F., Laurent-Charvet, S., 1999. A large-scale Palaeozoic dextral ductile strike-slip zone: the Aqqikkudug-Weiya zone along the northern margin of the Central Tianshan belt, Xinjiang, NW China. Acta Geological Sinica 73, 148–162.
Song, X.-Y., Chen, L.-M., Deng, Y.-F., Xie, W., 2013. Syn-collisional tholeiitic magmatism induced by asthenosphere upwelling due to slab detachment at the southern margin of the Central Asian Orogenic Belt. J. Geol. Soc., London 170, 941–950.
Song, X.-Y., Yi, J.-N., Chen, L.-M., She, Y.-W., Liu, C.-Z., Dang, X.-Y., Yang, Q.-A., Wu, S.-K., 2016. The giant Xiarihamu Ni-Co sulfide deposit in the East Kunlun Orogenic Belt, Northern Tibet Plateau, China. Econ. Geol. 111 (1), 29–55.
Song, X.Y., Deng, Y.F., Xie, W., Chen, L.M., Yu, S.Y., Liang, Q.L., 2018. Magmatism of Huangshan-Jingerquan Ni-Cu ore deposit belt and relationship with regional strike-slip structure in Xinjiang, China. J. Earth Sci. Environ. 40, 505–519 (in Chinese with English abstract).
Song, X.-Y., Deng, Y.-F., Xie, W., Yi, J.-N., Fu, B., Chen, L.-M., Yu, S.-Y., Zheng, W.-Q., Liang, Q.-L., 2021. Prolonged basaltic magmatism and short-lived magmatic sulfide mineralization in orogenic belts. Lithos 390-391, 106114.
Su, B.-X., Qin, K.-Z., Sakyi, P.A., Li, X.-H., Yang, Y.-H., Sun, H.e., Tang, D.-M., Liu, P.-P., Xiao, Q.-H., Malaviarachchi, S.P.K., 2011. U-Pb ages and Hf–O isotopes of zircons from Late Paleozoic mafic–ultramafic units in the southern Central Asian Orogenic Belt: tectonic implications and evidence for an Early-Permian mantle plume. Gondwana Res. 20 (2-3), 516–531.
Sun, S.-s., McDonough, W.F., 1989. Chemical and isotopic systematics of oceanic basalts: implications for mantle composition and processes. Geol. Soc., London, Special Publications 42 (1), 313–345.
Tang, M., Ji, W.Q., Chu, X., Wu, A.B., Chen, C., 2020. Reconstructing crustal thickness evolution from europium anomalies in detrital zircons. Geology 49, 76–80.
Utsunomiya, S., Valley, J.W., Cavosie, A.J., Wilde, S.A., Ewing, R.C., 2007. Radiation damage and alteration of zircon from a 3.3 Ga porphyritic granite from the Jack Hills, Western Australia. Chem. Geol. 236, 92–111.
Wang, B., Cluzel, D., Jahn, B.-m., Shu, L., Chen, Y., Zhai, Y., Branquet, Y., Barbanson, L., Sizaret, S., 2014. Late Paleozoic pre- and syn-kinematic plutons of the KangguerHuangshan shear zone: inference on the tectonic evolution of the Eastern Chinese North Tianshan. Am. J. Sci. 314 (1), 43–79.
Wang, F., Ge, C., Ning, S., Nie, L., Zhong, G., White, N., 2017. A new approach to LA-ICP-MS mapping and application in geology. Acta Petrologica Sinia 33, 3422–3436 (in Chinese with English abstract).
Wang, X., Griffin, W.L., Chen, J., Huang, P.Y., Li, X., 2011. U and Th contents and Th/U ratios of zircon in felsic and mafic magmatic rocks: improved zircon-melt distribution coefficients. Acta Geologica Sinica (English Edition) 85, 164–174.
Wang, X.S., Zhang, X., Gao, J., Li, J.L., Jiang, T., Xue, S.C., 2018. A slab break-off model for the submarine volcanic-hosted iron mineralization in the Chinese Western Tianshan: Insights from Paleozoic subduction-related to post-collisional magmatism. Ore Geol. Rev. 92, 144–160.
Wang, Y.u., Li, J., Sun, G., 2008. Postcollisional eastward extrusion and tectonic exhumation along the eastern Tianshan Orogen, Central Asia: constraints from dextral strike-slip motion and $^{40}Ar/^{39}Ar$ geochronological evidence. J. Geol. 116 (6), 599–618.
Wartes, M.A., Carroll, A.R., Greene, T.J., 2002. Permian sedimentary record of the Turpan-Hami basin and adjacent regions, northwest China: Constraints on postamalgamation tectonic evolution. Geol. Soc. Am. 114 (2), 131–152.
Watson, E.B., Harrison, T.M., 2005. Zircon thermometer reveals minimum melting conditions on earliest Earth. Science 308 (5723), 841–844.
Watson, E.B., Wark, D.A., Thomas, J.B., 2006. Crystallization thermometers for zircon and rutile. Contrib. Miner. Petrol. 151 (4), 413–433.
Wei, B., Wang, C.Y., Li, C., Sun, Y., 2013. Origin of PGE-depleted Ni-Cu sulfide mineralization in the Triassic Hongqiling No. 7 orthopyroxenite intrusion, Central Asian orogenic belt, northeastern China. Econ. Geol. 108 (8), 1813–1831.
White, L.T., Ireland, T.R., 2012. High-uranium matrix effect in zircon and its implications for SHRIMP U-Pb age determinations. Chem. Geol. 306–307, 78–91.
Williams, C.T., 1978. Uranium-enriched minerals in mesostasis areas of the Rhum layered pluton. Contrib. Miner. Petrol. 66 (1), 29–39.
Williams, I.S., Hergt, J.M., 2000. U-Pb dating of Tasmanian dolerites: a cautionary tale of SHRIMP analysis of high-U zircon. In: Beyond 2000: New Frontiers in Isotope Geoscience Abstract Proceedings, pp. 185–188.
Xiao, W.-J., Zhang, L.-C., Qin, K.-Z., Sun, S., Li, J.-L., 2004. Paleozoic accretionary and collisional tectonics of the Eastern Tianshan (China): implications for the continental growth of Central Asia. Am. J. Sci. 304, 370–395.
Xiao, W., Windley, B.F., Sun, S., Li, J., Huang, B., Han, C., Yuan, C., Sun, M., Chen, H., 2015. A tale of amalgamation of three Permo-Triassic collage systems in Central Asia: oroclines, sutures, and terminal accretion. Annu. Rev. Earth Planet. Sci. 43 (1), 477–507.
Xie, W., Song, X.-Y., Deng, Y.-F., Wang, Y.-S., Ba, D.-H., Zheng, W.-Q., Li, X.-B., 2012. Geochemistry and petrogenetic implications of a Late Devonian mafic-ultramafic intrusion at the southern margin of the Central Asian Orogenic Belt. Lithos 144, 209–230.
Xie, W., Xu, Y.G., Chen, Y.B., Luo, Z.Y., Hong, L.B., Ma, L., Liu, H.Q., 2016. High–alumina basalts from the Bogda Mountains suggest an arc setting for Chinese Northern Tianshan during the Late Carboniferous. Lithos 256–257, 165–181.
Xie, W., Lu, Y., Song, X.-Y., Deng, Y.-F., Liang, Q.-L., Yi, J.-N., 2022. A late Carboniferous bimodal volcanic suite before closure of the North Tianshan Ocean at the southwestern margin of the Central Asian Orogenic Belt. J. Asian Earth Sci. 226, 105090.
Xu, Y.G., Wei, X., Luo, Z.Y., Liu, H.Q., Cao, J., 2014. The Early Permian Tarim large igneous province: main characteristics and a plume incubation model. Lithos 204, 20–35.
Yakymchuk, C., Kirkland, C.L., Clark, C., 2018. Th/U ratios in metamorphic zircon. J. Metamorph. Geol. 36 (6), 715–737.
Yao, J.H., Zhu, W.G., Li, C., Zhong, H., Bai, Z.J., Ripley, E.M., Li, C., 2018. Petrogenesis and ore genesis of the lengshuiqing magmatic sulfide deposit in Southwest China: constraints from chalcophile elements (PGE, Se) and Sr-Nd-Os-S isotopes. Econ. Geol. 113, 675–698.
Yuan, C., Sun, M., Wilde, S., Xiao, W., Xu, Y., Long, X., Zhao, G., 2010. Postcollisional plutons in the Balikun area, East Chinese Tianshan: evolving magmatism in response to extension and slab break-off. Lithos 119 (3-4), 269–288.
Zhang, D.Y., Zhou, T.F., Yuan, F., Fan, Y., Deng, Y.F., Xu, C., Zhang, R.F., 2014. Genesis of Permian granites along the Kangguer Shear Zone, Jueluotage area, Northwest China: geological and geochemical evidence. Lithos 198, 141–152.
Zhao, L., Chen, H., Zhang, L., Zhang, W., Yang, J., Yan, X., 2018a. The Late Paleozoic magmatic evolution of the Aqishan-Yamansu belt, Eastern Tianshan: Constraints from geochronology, geochemistry and Sr–Nd–Pb–Hf isotopes of igneous rocks. J. Asian Earth Sci. 153, 170–192.
Zhao, Y., Xue, C.J., Zhao, X.B., Yang, Y.Q., Ke, J.J., 2015. Magmatic Cu-Ni sulfide mineralization of the huangshannan mafic-untramafic intrusion, Eastern Tianshan, China. J. Asian Earth Sci. 105, 155–172.

Zhao, Y., Xue, C.J., Symons, D., Zhao, X.B., Zhang, G.Z., Yang, Y.Q., Zu, B., 2018b. Temporal variations in the mantle source beneath the Eastern Tianshan nickel belt and implications for Ni-Cu mineralization potential. Lithos 314–315, 597–616.
Zhou, M.-F., Michael Lesher, C., Yang, Z., Li, J., Sun, M., 2004. Geochemistry and petrogenesis of 270 Ma Ni–Cu–(PGE) sulfide-bearing mafic intrusions in the Huangshan district, Eastern Xinjiang, Northwest China: implications for the tectonic evolution of the Central Asian orogenic belt. Chem. Geol. 209 (3-4), 233–257.
Zou, X.Y., Qin, K.Z., Han, X.L., Li, G.M., Evans, N.J., Li, Z.Z., Yang, W., 2019. Insight into zircon REE oxy-barometers: a lattice strain model perspective. Earth Planet. Sci. Lett. 506, 87–96.